lattice, and we only have to consider the effect of the excitation on the value of $U(x, y)$ and the range of the applicability of the continuum-wall approximation.[11]

The random displacement of the lattice atoms will make the periodicity of $U(x, y)$ less distinct and thus broaden the transverse-energy bands.

ACKNOWLEDGMENTS

Thanks are due to the Australian Research Grants Committee and to the Australian Institute of Nuclear Science and Engineering for support of this work.

*Deceased.

[1]J. Lindhard, Phys. Letters 12, 126 (1964); Kgl. Danske Videnskab. Selskab., Mat.-Fys. Medd. 34, 14 (1965).

[2]C. Erginsoy, Phys. Rev. Letters 15, 360 (1965).

[3]S. Datz, C. Erginsoy, G. Liebfried, and H. O. Lutz, Am. Rev. Nucl. Sci. 17, 129 (1967).

[4]L. T. Chadderton, J. Appl. Cryst. 3, 429 (1970).

[5]H. C. H. Nip and J. C. Kelly, Phys. Rev. B 5, 813 (1972).

[6]A. S. Davydov, *Quantum Mechanics* (Pergamon, New York, 1965).

[7]See, e.g., J. C. Slater, *Quantum Theory of Matter* (McGraw-Hill, New York, 1968).

[8]H. J. Kreiner, F. Bell, R. Sizman, D. Harder, and W. Huttl, Phys. Letters 33A, 135 (1970).

[9]H. C. H. Nip, R. L. Dalglish, A. P. M. Chang, and J. C. Kelly, Phys. Letters 34A, 257 (1971).

[10]Y. Kagan and Y. V. Kononets, Zh. Eksperim. i Teor. Fiz. 58, 226 (1970) [Sov. Phys. JETP 31, 124 (1970)].

[11]B. R. Appleton, L. C. Feldman, and W. L. Brown, BNL Report No. 5008, 1967, p. 45 (unpublished).

PHYSICAL REVIEW B VOLUME 5, NUMBER 5 1 MARCH 1972

Magnetic Circular Dichroism of Impurities in Solids: Vibrationally Induced $d \rightarrow d$ Transitions in MgO : Ni

B. D. Bird, G. A. Osborne, and P. J. Stephens*
Department of Chemistry, University of Southern California, Los Angeles, California 90007
(Received 28 June 1971)

We report absorption spectra and magnetic circular dichroism (MCD) of $d \rightarrow d$ transitions in single-crystal MgO:Ni over the range 4–300 °K. General theoretical expressions for the zeroth and first moments of the absorption and MCD of a vibration-induced band are derived. Their application to the MgO : Ni data leads to the conclusion that the intensities of the $^3T_1^a$, $^1T_2$, and $^3T_1^b$ bands are predominantly induced via t_{1u} vibrations. A consistent qualitative analysis of observed structure in these bands is made. The main vibrational structure is assigned to the dispersion of the allowing t_{1u} phonons. All spin-orbit components of the $^3T_1^a$ band are identified. The analysis does not require Jahn-Teller effects to be invoked in any of these bands.

I. INTRODUCTION

Magnetic circular dichroism (MCD) is being increasingly employed in the investigation of electronic spectra.[1,2] The principal uses of MCD in the study of impurities in crystals can be broadly categorized as follows: (i) determination of excited-state electronic properties, including symmetry, angular momentum, and spin-orbit splitting; (ii) elucidation of excited-state vibronic (electron-phonon) interactions; and (iii) detection of weak transitions. As yet, little application has been made to the $d \rightarrow d$ spectra of octahedrally coordinated transition-metal ions, probably for two reasons: Their gross features are already in many cases well interpreted, particularly for first-row ions, through ligand-field theory; and such transitions are frequently vibration induced (vibronically allowed, phonon assisted), complicating theoretical analysis. However, even for first-row ions at O_h sites in cubic crystals, there remain unidentified transitions and uncertainty in the interpretation of band fine structure. We have therefore initiated a study of the MCD of Co(II) and Ni(II) impurity ions in MgO and $KMgF_3$ lattices, systems already much investigated and important in the development of transition-metal spectroscopy.[3] We here report our preliminary findings for MgO : Ni. In Sec. II, the experimental results are presented. Expressions for the lower moments of the MCD and absorption of vibration-induced bands are then derived. Their application to the data leads to conclusions concerning the symmetries of the vibrations inducing the bands and to confirmation of the assignments of the transitions observed. Finally, the fine structure exhibited is discussed.

II. EXPERIMENTAL

Absorption spectra and MCD were measured with a Cary 14 and a Cary 61, respectively, as described in a previous paper.[4] Absorption measurements were made over the range 4–300 °K. MCD was

measured at Cary Instruments[5] with the collaboration of Duffield and Abu-Shumays. Fields of 0–50 kG were used, generated by a Varian Associates superconducting magnet. Measurements were made at temperatures between 4 and 300 °K, different temperatures in the range 4–77 °K being obtained by varying thermal contact between the sample holder and the magnet Dewar and by incorporating a cupron heater, operated by a variac, in the crystal holder.

The MgO : Ni crystal was obtained from Semi-Elements, Inc., and, after polishing, had a 4.8-mm path length between 5.5×6.5-mm 001 faces. The effects of strain, both intrinsic to the crystal and induced by mounting, were examined in the room-temperature and one low-temperature experiment by measuring the circular dichroism (CD) of solutions of *D*-*ddd*-cobalt trispropylenediamine chloride and copper *L*-proline, with and without the crystal mounted in series. No distortion of the natural CD signal by the crystal was observed, consistent with the negligible strain exhibited when viewed between crossed polarizers. Errors in the MCD data due to crystal imperfection can therefore be ignored.

The dependence of MCD on field strength H and direction was investigated. No nonlinearities were detected up to 50 kG.

Selected absorption and MCD data are shown in Figs. 1–7. A is absorbance and $\Delta A = A_L - A_R$. In all cases except the 8005- and 8182-cm^{-1} lines the spectra are fully resolved. MCD data are normalized to + 10 kG (positive fields pointing in the direction of light propagation). Spectra are shown in most cases after subtraction of background baselines. In all MCD spectra these were straight lines, and this is also the case for the 9000- and 15 000-cm^{-1} absorption bands. The 22 000-cm^{-1} band is superimposed on the low-energy tail of the 25 000-cm^{-1} band and is shown in Fig. 4 without subtraction of this background. The 25 000-cm^{-1} band also merges into the tail of absorption, presumably charge transfer, at higher energies. Spectra in Fig. 6 are shown after subtraction of this background, estimated by fitting the higher-energy region, assuming a double-Gaussian dispersion. The background is also shown at one temperature.

Some moments of the absorption and MCD data are given in Figs. 8–10 and Table I. Moments are defined through

$$\langle A \rangle_n^{\nu^0} = \int \frac{A}{\nu} (\nu - \nu^0)^n d\nu \ , \qquad \langle \Delta A \rangle_n^{\nu^0} = \int \frac{\Delta A}{\nu} (\nu - \nu^0)^n d\nu \ , \tag{1}$$

where ν is in cm^{-1} and ν^0 is the average frequency, making $\langle A \rangle_1^{\nu^0} = 0$, MCD moments are normalized to + 10 kG, and integration is over an entire resolved band. Moments are evaluated after subtraction of backgrounds as described above. Absorption moments of the 22 000-cm^{-1} band were obtained at low temperatures assuming a straight background, but not at higher temperatures, owing to the difficulty of removing the 25 000-cm^{-1} band tail satisfactorily.

In addition to the data discussed above, various very weak bands were observed in either absorption or MCD, or both. None of these have been definitely identified as transitions of single Ni^{2+} ions and further experiments are required to establish their origin. These bands are therefore not discussed in detail here.

The Ni concentration in the crystal has not been

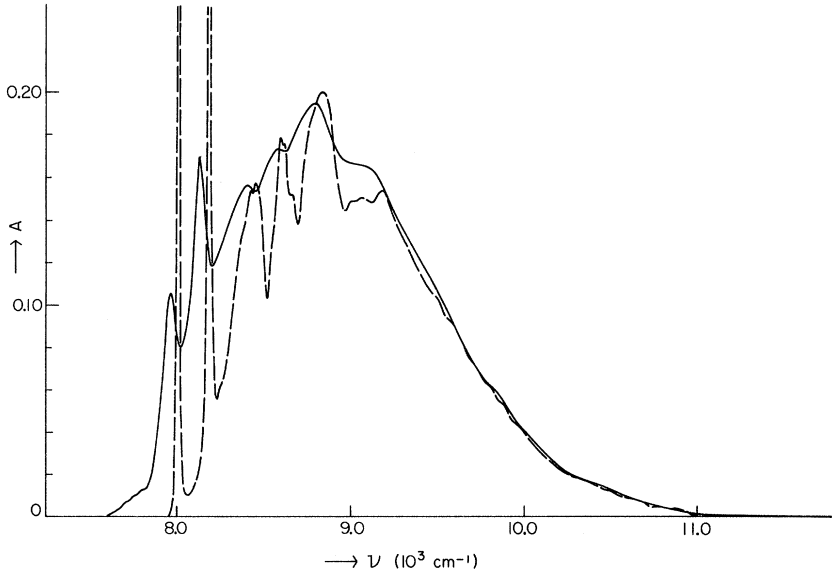

FIG. 1. Absorption spectrum of $^3T_2$ band of MgO : Ni; long-dashed line, 79 °K; solid line, 208 °K. Straight baselines have been subtracted.

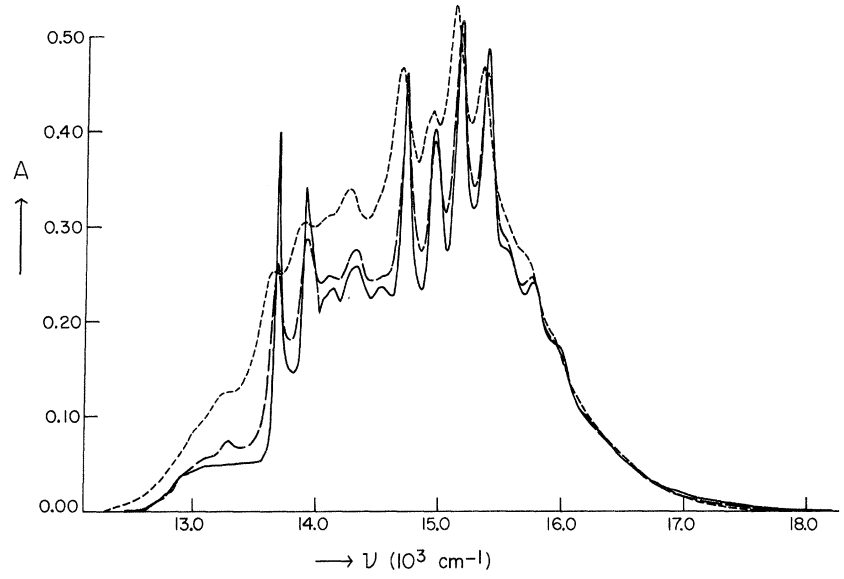

FIG. 2. Absorption spectrum of $^3T_1^a$ band of MgO : Ni; solid line, 8 °K; long-dashed line, 130 °K; short-dashed line, 222 °K. Straight baselines have been subtracted.

measured. However, comparison with the absorption spectra of Pappalardo, Wood, and Linares[6] on a crystal of known concentration leads to an estimated Ni/Mg ratio of $2-3\times10^{-3}$. With this value, f numbers for the absorption bands are $\sim 4\times10^{-8}\nu^0\langle A\rangle_0$.

III. MOMENT ANALYSIS FOR VIBRATION-INDUCED TRANSITIONS

In this section we derive expressions for the zeroth and first moments of the absorption and MCD

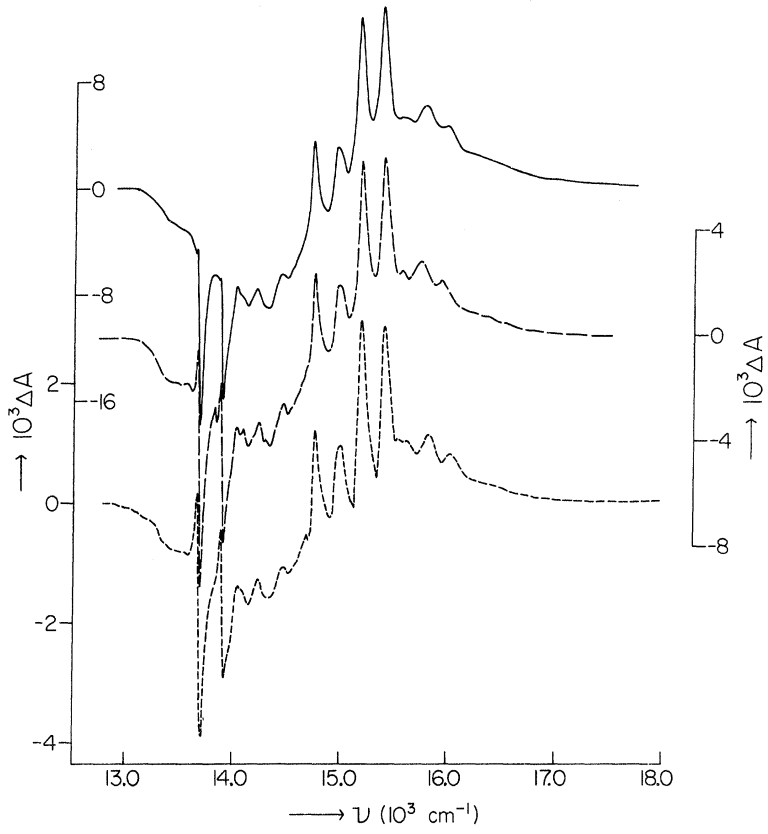

FIG. 3. MCD of $^3T_1^a$ band of MgO : Ni normalized to $H=10$ kG. Solid line, 18 °K (upper left-hand scale); long-dashed lines, 44 °K (right-hand scale); short-dashed line, 95 °K (lower left-hand scale). Straight baselines have been subtracted.

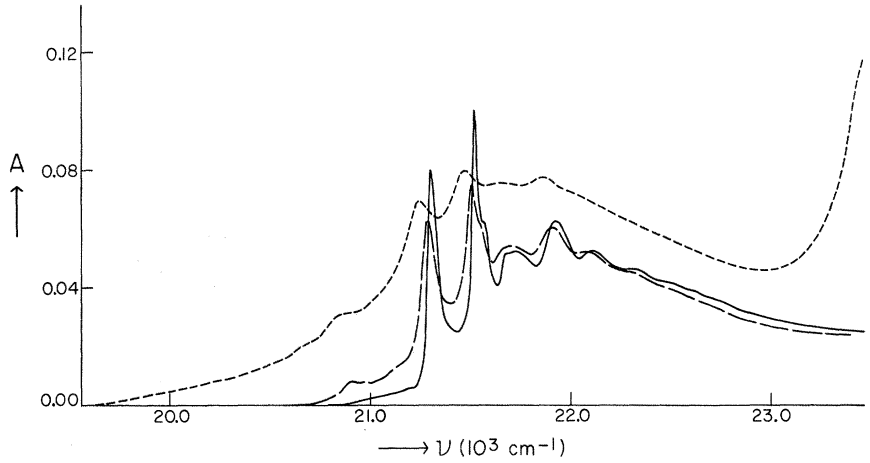

FIG. 4. Absorption spectrum of $^1\Gamma$ band of MgO : Ni; solid line, 8 °K; long-dashed line, 121 °K; short-dashed line, 208 °K. Flat baselines have been subtracted.

due to vibration-induced electric dipole transitions of impurities in crystals. The method and notation follow those of previous papers.[4,7]

From Eqs. (5) and (33)–(35) of Ref. 4 we have, for the $A \rightarrow J$ absorption band comprising transitions between ground and excited continua of zero-field levels (a and j),

$$\langle A \rangle_n^{\nu^0} = 1.089\times10^2\left(\frac{\alpha^2}{n}\right)\mathfrak{D}_n^{\nu^0} cz \ ,$$

$$\frac{\langle \Delta A \rangle_n^{\nu^0}}{\langle A \rangle_0} = \frac{-0.934(\mathfrak{A}_n^{\nu^0} + \mathfrak{B}_n^{\nu^0} + \mathfrak{C}_n^{\nu^0}/kT)}{\mathfrak{D}_0} \ , \qquad (2)$$

where c is the concentration in moles/liter, z is the path length in cm, α^2/n is the effective field correction factor, kT is in cm^{-1}, $\langle \Delta A \rangle_n^{\nu^0}$ is normalized to + 10 kG, and *inter alia* ,

$$\mathfrak{D}_n^{\nu^0} = \frac{3}{4}\sum_{a,j}\frac{N_a}{N_A}\left[|\langle a|m_-|j\rangle|^2(\nu_{ja}-\nu^0)^n + \text{v.v.}\right] \ ,$$

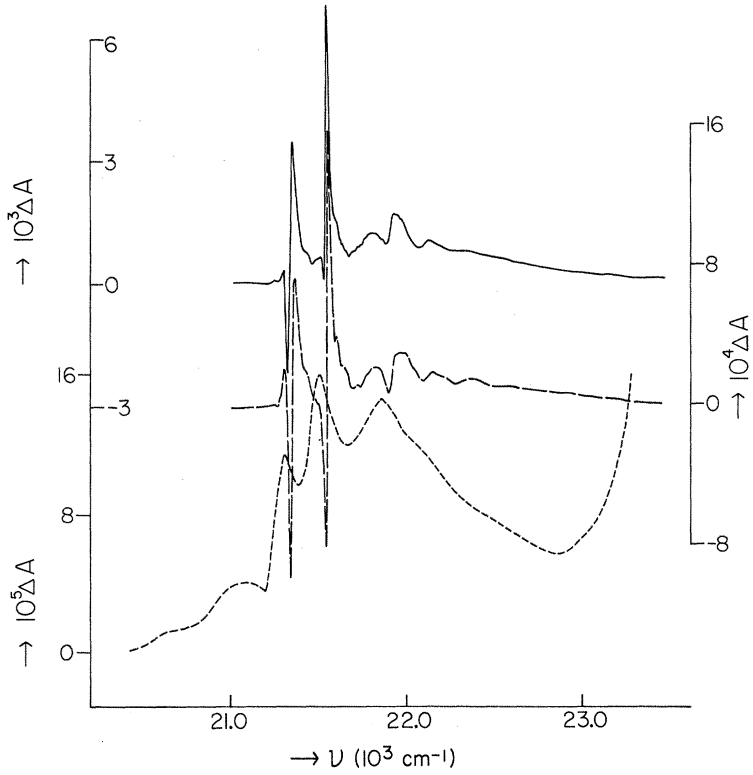

FIG. 5. MCD of $^1\Gamma$ band of MgO : Ni normalized to $H = 10$ kG. Solid line, 18 °K (upper left-hand scale); long-dashed line, 93 °K (right-hand scale); short-dashed line, 300 °K (lower left-hand scale). Straight baselines have been subtracted.

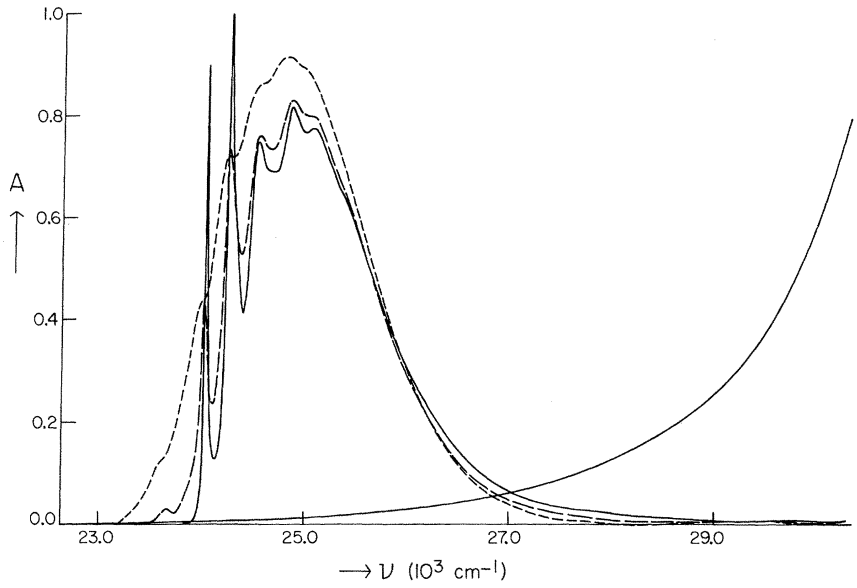

FIG. 6. Absorption spectrum of $^3T_1^b$ band of MgO : Ni; solid line, 8 °K; long-dashed line, 121 °K; short-dashed line, 208 °K. Curved baselines have been subtracted; that for the 8 °K spectrum is shown.

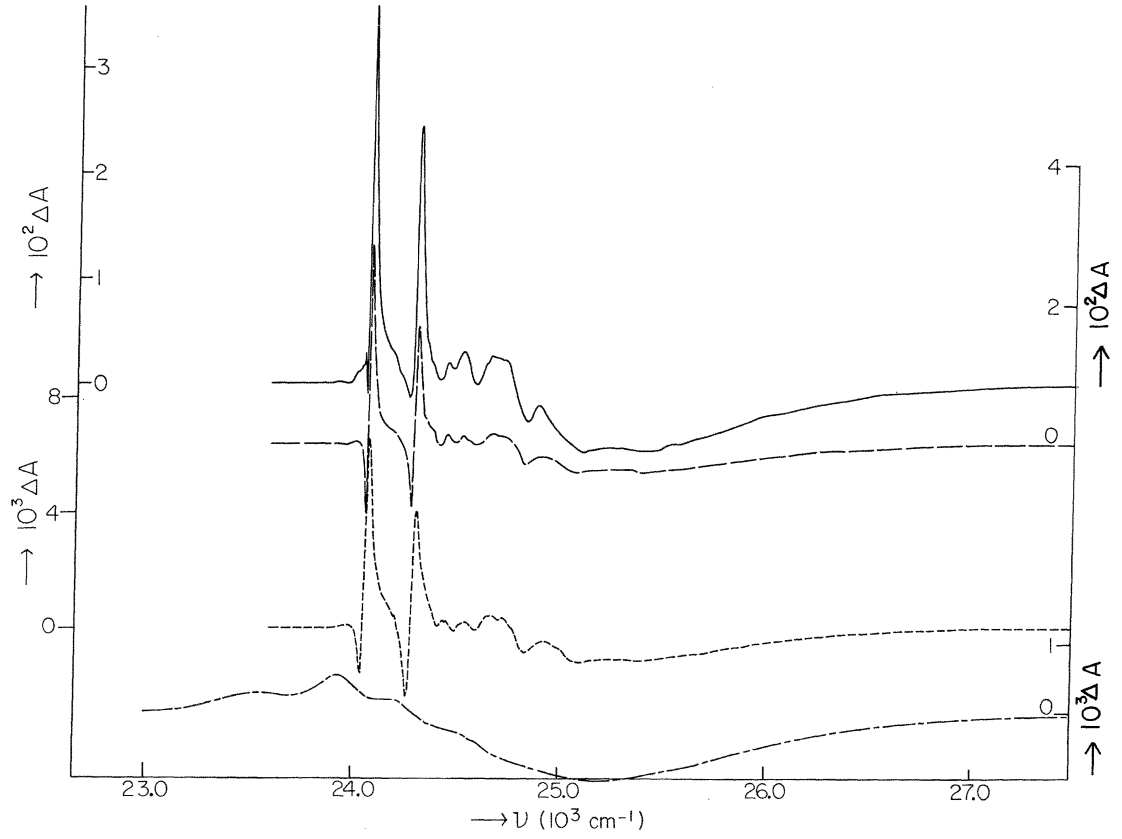

FIG. 7. MCD of $^3T_1^b$ band of MgO : Ni normalized to $H = 10$ kG. Solid line, 18 °K (upper left-hand scale); long-dashed line, 45 °K (upper right-hand scale); short-dashed line, 91 °K (lower left-hand scale); long/short dashed line, 300 °K (lower right-hand scale). Straight baselines have been subtracted.

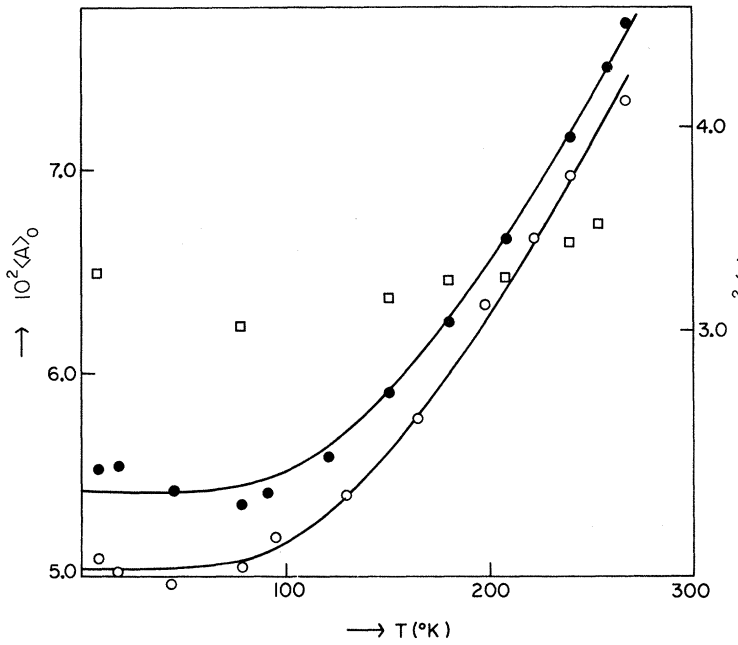

FIG. 8. $\langle A\rangle_0$: open square, ${}^3T_2$ band (RH scale); open circle, ${}^3T_1^a$ band; closed circle, ${}^3T_1^b$ band (left-hand scale). Full lines represent the equation $\langle A\rangle_0 = \langle A\rangle_0^0 \times \coth(\hbar\omega/2kT)$ with $\langle A\rangle_0^0 = 5.04\times10^{-2}$, $\hbar\omega = 308$ cm^{-1} (lower line) and $\langle A\rangle_0^0 = 5.42\times10^{-2}$, $\hbar\omega = 329$ cm^{-1} (upper line).

$$\mathfrak{a}_1^{\nu 0} = \frac{3}{4}\sum_{a,j,j'}\frac{N_a}{N_A}[\langle a|m_-|j\rangle\langle\langle j|\mu_z|j'\rangle - \langle a|\mu_z|a\rangle\delta_{jj'}) \times\langle j'|m_+|a\rangle - \text{v. v.}], \quad (3)$$

$$\mathfrak{e}_n^{\nu 0} = -\frac{3}{4}\sum_{a,j}\frac{N_a}{N_A}[\langle a|\mu_z|a\rangle|\langle a|m_-|j\rangle|^2(\nu_{ja}-\nu^0)^n - \text{v. v}].$$

Here, N_a/N_A is the occupation probability of state a, $\vec{m}$ and $\vec{\mu}$ are the electronic electric and magnetic dipole operators in Debye and Bohr magneton units, respectively, $m_\pm \equiv m_x \pm i m_y$, ν_{ja} is the separation in cm^{-1} of states j and a, and v. v. indicates the repetition of previous terms with m_+ and m_- interchanged. In deriving Eqs. (2) and (3) it is assumed that the

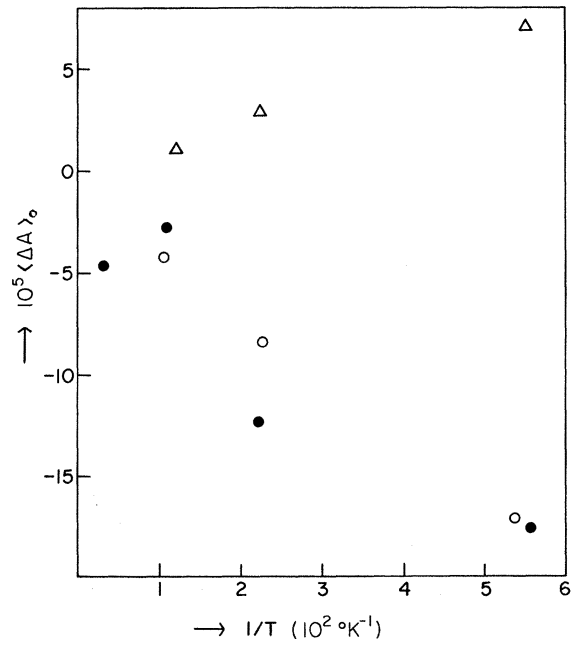

FIG. 9. $\langle\Delta A\rangle_0$, normalized to $H = 10$ kG. Open circle, ${}^3T_1^a$ band; open triangle, ${}^1\Gamma$ band; closed circle, ${}^3T_1^b$ band.

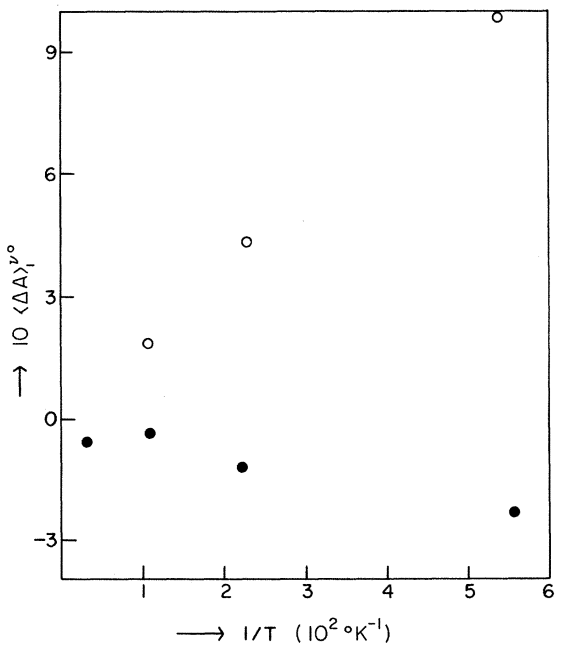

FIG. 10. $\langle\Delta A\rangle_1^{\nu 0}$, normalized to $H = 10$ kG. Open circle, ${}^3T_1^a$ band; closed circle, ${}^3T_1^b$ band.

impurity absorption is localized and electric dipole, that the Zeeman perturbation $\mathcal{H}_0' = -\mu_z H$ is diagonal within the $|a\rangle$ manifold, and that kT is large compared to ground-state Zeeman energies (when saturation effects can be ignored).

We now assume that the ground electronic states A_α ($\alpha = 1 - d_A$) possess a single harmonic potential surface with vibronic levels described by the Born-Oppenheimer (BO) approximation

$$W_{A_\alpha} = \langle \psi_{A_\alpha} | \mathcal{H}_e^0 | \psi_{A_\alpha} \rangle = W_A^0 + \tfrac{1}{2} \sum_i k_A^i q_i^2 \quad (k_A^i = \omega_i^2) , \tag{4}$$

$$|a\rangle = \psi_{A_\alpha} \chi_a ,$$

where $\mathcal{H}_e^0 = \mathcal{H} - T_n$ is the electronic Hamiltonian, $\mathcal{H}$ being the complete zero-field Hamiltonian and T_n the nuclear kinetic-energy operator, and q_i are mass-normalized normal coordinates (infinite in number) for the impurity-crystal system. The excited levels are supposed to belong to a set of electronic states J_λ ($\lambda = 1 - d_J$) with wave functions ψ_{J_λ} and to be described by the BO approximation, generalized to near-degenerate states. It is useful to introduce the functions ϕ_{J_λ}, related to ψ_{J_λ} through a unitary transformation:

$$\psi_{J_\lambda} = \sum_{\lambda'} C_{\lambda\lambda'} \phi_{J_{\lambda'}} , \tag{5}$$

where $C_{\lambda\lambda'}$ is a function of nuclear coordinates and is chosen to make ϕ_{J_λ} vary slowly with nuclear displacements q_i. Then, assuming $\langle \psi_{A_\alpha} | \vec{m} | \psi_{J_\lambda} \rangle = 0$ at $\vec{R}_0$, the ground-state equilibrium geometry (all $q_i = 0$), so that the $A \rightarrow J$ transitions are entirely vibration induced, and expanding matrix elements of $\vec{m}$ and $\vec{\mu}$ in powers of q, we have to lowest order

$$\begin{aligned} &\langle \psi_{A_\alpha} | \vec{m} | \phi_{J_\lambda} \rangle = \textstyle\sum_i \vec{m}_i^{\alpha\lambda} q_i , \\ &\langle \psi_{A_\alpha} | \mu_z | \psi_{A_{\alpha'}} \rangle = \langle A_\alpha | \mu_z | A_{\alpha'} \rangle , \\ &\langle \phi_{J_\lambda} | \mu_z | \phi_{J_{\lambda'}} \rangle = \langle J_\lambda | \mu_z | J_{\lambda'} \rangle , \end{aligned} \tag{6}$$

where $\langle A_\alpha | \mu_z | A_{\alpha'} \rangle \equiv \langle \psi_{A_\alpha}(\vec{R}_0) | \mu_z | \psi_{A_{\alpha'}}(\vec{R}_0) \rangle$ and so on. To the same order as Eq. (4)

$$\langle \phi_{J_\lambda} | \mathcal{H}_e^0 | \phi_{J_{\lambda'}} \rangle = W_J^0 \delta_{\lambda\lambda'} + w_{\lambda\lambda'}^0 + \sum_i l_{\lambda\lambda'}^i q_i + \tfrac{1}{2} \sum_{i,j} k_{\lambda\lambda'}^{ij} q_i q_j \tag{7}$$

from which

$$\langle \phi_{J_\lambda} | \mathcal{H}_e^0 | \phi_{J_{\lambda'}} \rangle - \langle \psi_{A_\alpha} | \mathcal{H}_e^0 | \psi_{A_\alpha} \rangle \delta_{\lambda\lambda'} = W_{JA}^0 \delta_{\lambda\lambda'} + w_{\lambda\lambda'}^0 + \sum_i l_{\lambda\lambda'}^i q_i + \tfrac{1}{2} \sum_{i,j} \kappa_{\lambda\lambda'}^{ij} q_i q_j , \tag{8}$$

where $W_{JA}^0 = W_J^0 - W_A^0$ and $\kappa_{\lambda\lambda'}^{ij} = k_{\lambda\lambda'}^{ij} - k_A^i \delta_{\lambda\lambda'} \delta_{ij}$. Then diagonalizing $\langle A_\alpha | \mu_z | A_{\alpha'} \rangle$,[8] substitution in Eq. (3) leads to

$$\begin{aligned} &\mathfrak{D}_0 = \sum_{\alpha\lambda i} (d_i^{\alpha\lambda\lambda} + \text{v. v.}) \Omega_i , \\ &\nu^0 = W_{JA}^0 + \sum_{\alpha\lambda i} (d_i^{\alpha\lambda\lambda} + \text{v. v.}) \hbar\omega_i / \sum_{\alpha\lambda i} (d_i^{\alpha\lambda\lambda} + \text{v. v.}) \Omega_i + \sum_{\alpha\lambda\lambda' i} (d_i^{\alpha\lambda\lambda'} w_{\lambda\lambda'}^0 + \text{v. v.}) \Omega_i / \sum_{\alpha\lambda i} (d_i^{\alpha\lambda\lambda} + \text{v. v.}) \Omega_i + O(\kappa) \equiv W_{JA}^0 + \delta , \\ &\mathfrak{A}_1 = \sum_{\alpha\lambda\lambda' i} [d_i^{\alpha\lambda\lambda'} (\langle J_\lambda | \mu_z | J_{\lambda'} \rangle - \langle A_\alpha | \mu_z | A_\alpha \rangle \delta_{\lambda\lambda'}) - \text{v. v.}] \Omega_i , \\ &\mathfrak{C}_0 = -\sum_{\alpha\lambda i} (d_i^{\alpha\lambda\lambda} \langle A_\alpha | \mu_z | A_\alpha \rangle - \text{v. v}) \Omega_i , \\ &\mathfrak{C}_1^{\nu 0} = -\sum_{\alpha\lambda\lambda' i} (d_i^{\alpha\lambda\lambda'} \langle A_\alpha | \mu_z | A_\alpha \rangle - \text{v. v}) [\hbar\omega_i \delta_{\lambda\lambda'} + w_{\lambda\lambda'}^0 \Omega_i + O(\kappa)] - \delta \mathfrak{C}_0 , \\ &d_i^{\alpha\lambda\lambda'} = (3\hbar^2 / 8 d_A)(m_{-i}^{\alpha\lambda} m_{+i}^{\lambda'\alpha}) (\hbar\omega_i)^{-1} , \\ &\Omega_i = \coth(\hbar\omega_i / 2kT) , \end{aligned} \tag{9}$$

where W_{JA}^0, δ, $w_{\lambda\lambda'}^0$, $\hbar\omega_i$, and kT are in cm^{-1} and $O(\kappa)$ indicates terms in $\kappa_{\lambda\lambda'}^{ij}$.

The coefficients $\vec{m}_i^{\alpha\lambda}$ of Eq. (6) and the parameters of Eqs. (7) and (8) will often be obtained by perturbation theory. For example, when all J_λ states are degenerate at $\vec{R}_0$, choosing $C_{\lambda\lambda'}(\vec{R}_0) = \delta_{\lambda\lambda'}$ leads to

$$\vec{m}_i^{\alpha\lambda} = \sum_{X \neq J} \langle A_\alpha | \vec{m} | X \rangle \langle X | u_i | J_\lambda \rangle / W_J^0 - W_X^0 + \sum_{X \neq A} \langle A_\alpha | u_i | X \rangle \langle X | \vec{m} | J_\lambda \rangle / W_A^0 - W_X^0 , \tag{10}$$

where $u_i = (\partial \mathcal{H}_e^0 / \partial q_i)_{\vec{R}_0}$ and $\langle A_\alpha | \vec{m} | X \rangle \equiv \langle \psi_{A_\alpha}(\vec{R}_0) | \vec{m} | \psi_X(\vec{R}_0) \rangle$ and so on. Calculation of W_{JA}^0, $w_{\lambda\lambda'}^0$, $l_{\lambda\lambda'}^i$, and $\kappa_{\lambda\lambda'}^{ij}$ using perturbation theory in this and more complex situations was discussed previously.[4]

IV. DISCUSSION

The three main bands observed in the MgO : Ni spectrum arise from the $^3T_2$, $^3T_1^a$, and $^3T_1^b$ excited levels,[9] respectively. The weaker band at 22 000 cm^{-1} therefore involves singlet excited states $^1\Gamma$. The results of a "complete" ligand-field calculation[10] with $\Delta = 8763$, $B = 860$, $C = 3570$, and $\zeta = 550$ cm^{-1} are given in Table II and show that, for these or any other reasonable parameters, $^1\Gamma$ can only be $^1T_2$ or $^1A_1$, or both. With these parameters the lowest ^1E and $^1T_1$ states lie, respectively, just below and above the $^3T_1^a$ and $^3T_1^b$ manifolds and the remaining

TABLE I. Experimental parameters.

Band	T (°K)	$\langle A\rangle_0$[a]		$\langle\Delta A\rangle_0$[b]	ν^0 (cm^{-1})	$\langle\Delta A\rangle_1^{\nu^0}$[b]	$\frac{\langle\Delta A\rangle_0 kT}{\langle A\rangle_0}$[b,c]	$\frac{\langle\Delta A\rangle_1^{\nu^0} kT}{\langle A\rangle_0}$[b,c]	$\frac{\mathcal{C}_0}{\mathfrak{D}_0}$[d]	$\frac{\mathcal{C}_1}{\mathfrak{D}_0}$[d]
	18	5.02×10^{-2}	(1.00)	-17.1×10^{-5}	14868	9.82×10^{-1}	-4.43×10^{-2}	254		
$^3T_1^a$	44	4.97×10^{-2}		-8.36×10^{-5}	14854	4.38×10^{-1}	-5.16×10^{-2}	270		
	95	5.19×10^{-2}		-4.22×10^{-5}	14850	1.88×10^{-1}	-5.38×10^{-2}	240		
						Average:	-4.99×10^{-2}	255	5.34×10^{-2}	-273
	18	2.67×10^{-3}	(0.053)	7.03×10^{-5}			3.34×10^{-1}			
$^1\Gamma$	45	2.72×10^{-3}		2.95×10^{-5}			3.38×10^{-1}			
	93	2.65×10^{-3}		1.22×10^{-5}			2.99×10^{-1}			
						Average:	3.24×10^{-1}		-3.47×10^{-1}	
	18	5.54×10^{-2}	(1.104)	-17.6×10^{-5}	25254	-2.31×10^{-1}	-4.00×10^{-2}	-52.5		
$^3T_1^b$	45	5.42×10^{-2}		-12.3×10^{-5}	25221	-1.20×10^{-1}	-7.15×10^{-2}	-69.7		
	91	5.41×10^{-2}		-2.75×10^{-5}	25156	-3.78×10^{-2}	-3.23×10^{-2}	-44.4		
						Average:	-4.79×10^{-2}	-55.5	5.13×10^{-2}	59.4

[a]Numbers in parentheses give values relative to $^3T_1^a$ band $\langle A\rangle_0$ at 18 °K.
[b]$\langle\Delta A\rangle_n^{\nu^0}$ values normalized to $H=+10$ kG.
[c]kT in cm^{-1}.
[d]Obtained using Eq. (2).

singlet states occur somewhat above $^3T_1^b$. These states are not clearly distinguishable in the spectra.

The $\langle A\rangle_0$ values of the $^3T_1^a$, $^3T_1^b$, and $^1\Gamma$ bands increase substantially with T and, in the first two cases,[11] can be fitted to the form

$$\langle A\rangle_0(T)=\langle A\rangle_0^0\coth(\hbar\omega/2kT)\,, \tag{11}$$

as shown in Fig. 8. These bands thus appear to be entirely vibration induced. The $^3T_2$ band, on the other hand, shows a much smaller T dependence. This can be attributed to a major T-independent allowed magnetic dipole contribution. Using the expression

$$\langle A\rangle_0=9.36\times10^{-3}cz\left(\frac{3}{d_A}\right)\sum_{\alpha,\lambda}|\langle A_\alpha|\mu_z|J_\lambda\rangle|^2 \tag{12}$$

TABLE II. Calculated parameters.

	State	Energy (cm^{-1})	Magnetic dipole intensity[a]	$\mathfrak{D}_0(\Lambda)$[b]	$\mathfrak{D}_0$[b]	$\mathcal{C}_0(\Lambda)$[b]	$\mathcal{C}_0$[b]	$\frac{\mathcal{C}_0}{\mathfrak{D}_0}$	$\frac{\mathcal{C}_1}{\mathfrak{D}_0}$
$^3A_2$	T_2	0							
	E	8512	0.245	0.0026		-0.0014			
$^3T_2$	T_1	8650	0.364	0.0021	0.007	0.0012			
	T_2	8978	0.300	0.0019		-0.0011			
	A_2	9118	0.091	0		0			
	E[c]	13346	1.1×10^{-3}	0.0496		-0.0275			
	A_1	13780	0	0.1033		0.1144			
	T_1	14196	4.5×10^{-4}	0.3198		0.2045			
$^3T_1^a$	T_2	14842	3.0×10^{-4}	0.3464	1.00	-0.1918	-0.0005	-0.0005	-250
	E	15225	11.1×10^{-4}	0.1808		-0.1001			
	T_2[c]	21790	5×10^{-6}	0.0256		-0.0142		-0.555	
	A_1[c]	22300	0	0.0000		0.0000			
	E	24705	7×10^{-5}	0.1732		-0.0959			
$^3T_1^b$	T_2	24924	4×10^{-5}	0.2358	0.80	-0.1305	$+0.0437$	0.055	86
	T_1	25035	3×10^{-5}	0.2865		0.1586			
	A_1	25204	0	0.0999		0.1106			
	T_1[c]	26339	2×10^{-5}	0.0017		0.0010			
	E[1]	32991	2×10^{-6}	0.0007		-0.0005			
	T_2[c]	33362	2×10^{-6}	0.0005		-0.0003			
	A_1[c]	56846	0	0.0002		0.0002			

[a]Values given are $\sum_{\alpha,\lambda}|\langle A_\alpha|\mu_z|J_\lambda\rangle|^2/11.88$, making the total $^3T_2$ intensity = 1.
[b]Units $0.813\ [\sum_i M_i^2\hbar^2(2\hbar\omega_i)^{-1}\coth(\hbar\omega_i/2kT)]$.
[c]Predominantly singlet state.

and a concentration of 0.25 at. %, we calculate the magnetic dipole $\langle A \rangle_0$ to be 1.2×10^{-2}, consistent with this conclusion. The vibration-induced intensity in the $^3T_2$ band is thus much smaller than in the $^3T_1$ bands. The magnetic dipole intensities were also calculated for all other bands, as shown in Table II. The ratio to the $^3T_2$ band intensity nowhere exceeds 2×10^{-3} and contributions to the observed $^3T_1^a$, $^3T_1^b$, and $^1\Gamma$ band over-all intensities are thus clearly negligible, in agreement with the conclusion reached above.

We now discuss the $^3T_1^a$, $^3T_1^b$, and $^1\Gamma$ band absorption and MCD zeroth and first moments, assuming them to be entirely vibration induced and using the results of Sec. III. The MCD moments up to 100 °K are linear in $1/T$ within experimental error, as shown in Figs. 9 and 10. They can therefore be attributed entirely to $\mathcal{C}$ terms and only these are considered. To begin with we assume that vibrations of only t_{1u} symmetry are active in producing intensity; other symmetries are considered later. We define

$$\mathcal{H}_e^0 = \mathcal{H}_0 + \mathcal{H}'_{\rm so} , \tag{13}$$

where $\mathcal{H}'_{\rm so}$ is the spin-orbit interaction, and assume $\mathcal{H}'_{\rm so}(q) = \mathcal{H}'_{\rm so}(\vec{R}_0)$. At $\vec{R}_0$, ligand-field theory gives

$$\begin{aligned}\psi_{A_\alpha}(\vec{R}_0) &= |T_2\alpha\rangle = \sum_{S\Gamma} |S\Gamma T_2\alpha\rangle\langle S\Gamma T_2\alpha|T_2\alpha\rangle ,\\ \psi_{J_\lambda}(\vec{R}_0) &= |\Lambda\lambda\rangle = \sum_{S\Gamma} |S\Gamma\Lambda\lambda\rangle\langle S\Gamma\Lambda\lambda|\Lambda\lambda\rangle ,\end{aligned} \tag{14}$$

where Λ designates a spin-orbit representation, the expansions are over Russell-Saunders strong-field functions, Λ runs over spin-orbit states contributing to the J manifold, and we choose α to diagonalize $\langle A_\alpha|\mu_z|A_\alpha\rangle$. Choosing ϕ_{J_λ} functions to reduce to ψ_{J_λ} at $\vec{R}_0$ then leads to

$$\vec{m}_i^{\alpha,\Lambda\lambda} = \sum_{S\Gamma;S'\Gamma'} \langle T_2\alpha|S\Gamma T_2\alpha\rangle \vec{M}_i^{S\Gamma T_2\alpha, S'\Gamma'\Lambda\lambda} \langle S'\Gamma'\Lambda\lambda|\Lambda\lambda\rangle , \tag{15}$$

where

$$\begin{aligned}\vec{M}_i^{S\Gamma T_2\alpha, S'\Gamma'\Lambda\lambda} = \Bigg(&\sum_{X\neq\Lambda} \langle S\Gamma T_2\alpha|\vec{m}|X\rangle\langle X|u_i|S'\Gamma'\Lambda\lambda\rangle/W_\Lambda^0 - W_X^0\\ &+ \sum_{X\neq T_2} \langle S\Gamma T_2\alpha|u_i|X\rangle\langle X|\vec{m}|S'\Gamma'\Lambda\lambda\rangle/W_{T_2}^0 - W_X^0\Bigg),\end{aligned} \tag{16}$$

where $u_i = (\partial\mathcal{H}_0/\partial q_i)_{\vec{R}_0}$ and all matrix elements are evaluated at $\vec{R}_0$. The dominant contributor to the ground state is the $^3A_2(t_2^6e^2)$ function and we approximate $\vec{m}_i^{\alpha,\Lambda\lambda}$ by considering only terms with $S\Gamma = {}^3A_2$ (when $\alpha = M_S$). The quantities $\vec{M}_i^{^3A_2M_S, S'\Gamma'\Lambda\lambda}$ are those responsible for the spin-allowed band intensities in the limit $\mathcal{H}'_{\rm so} = 0$. As shown above, the $^3T_2$ band has much smaller vibration-induced intensity than the $^3T_1$ bands and we therefore also neglect terms with $S'\Gamma' = {}^3T_2$. Since u_i and $\vec{m}$ are one-electron operators it follows that of the $t_2^5e^3$ and $t_2^4e^4$ $^3T_1$ functions only the former contributes. With the further approximation that $W_\Lambda^0 = W_T^0$ Eq. (15) then reduces to

$$\vec{m}_i^{M_S,\Lambda\lambda} = \langle T_2|{}^3A_2\rangle \vec{M}_i^{M_S,\Lambda\lambda} \langle 53|\Lambda\rangle , \tag{17}$$

where

$$\begin{aligned}\vec{M}_i^{M_S,\Lambda\lambda} = (&\textstyle\sum_X \langle {}^3A_2M_S|\vec{m}|X\rangle\langle X|u_i|{}^3T_1^{53}\Lambda\lambda\rangle/W_T^0 - W_X^0\\ &+ \textstyle\sum_X \langle {}^3A_2M_S|u_i|X\rangle\langle X|\vec{m}|{}^3T_1^{53}\Lambda\lambda\rangle/W_{^3A_2}^0 - W_X^0) ,\end{aligned} \tag{18}$$

and $\langle T_2|{}^3A_2\rangle = \langle T_2\alpha|{}^3A_2M_S\rangle$ and $\langle 53|\Lambda\rangle = \langle {}^3T_1^{53}\Lambda\lambda|\Lambda\lambda\rangle$.

It is convenient here to define the quantities

$$\begin{aligned} d_{i\Lambda} &= \sum_{M_S,\Lambda,\beta} (|M_{-i\beta}^{M_S,\Lambda\lambda}|^2 + \text{v. v.}) ,\\ c_{i\Lambda} &= \sum_{M_S,\lambda,\beta} (|M_{-i\beta}^{M_S,\Lambda\lambda}|^2 - \text{v. v.})\, M_S ,\end{aligned} \tag{19}$$

where $i\beta$ denotes the β component of the ith t_{1u} mode. Using group theory, $d_{i\Lambda}$ and $c_{i\Lambda}$ can be expressed in terms of a single constant

$$d_{i\Lambda} = d_\Lambda M_i^2 , \quad c_{i_\Lambda} = c_\Lambda M_i^2 , \tag{20}$$

where

$$\begin{array}{cccc}\Lambda = A_1 , & d_\Lambda = \frac{2}{3} , & c_\Lambda = \frac{1}{3}\\ E & \frac{4}{3} & -\frac{1}{3}\\ T_1 & 2 & \frac{1}{2}\\ T_2 & 2 & -\frac{1}{2} .\end{array} \tag{21}$$

Substituting in Eq. (9) then leads to

$$\begin{aligned}&\mathfrak{D}_0 = \textstyle\sum_\Lambda \mathfrak{D}_0(\Lambda), \quad \mathfrak{C}_0 = \textstyle\sum_\Lambda \mathfrak{C}_0(\Lambda),\\ &\mathfrak{C}_1^{\nu 0} = \textstyle\sum_\Lambda \mathfrak{C}_0(\Lambda)(w_\Lambda^0 - \epsilon) ,\\ &\mathfrak{D}_0(\Lambda) = \tfrac{1}{4}\langle T_2|{}^3A_2\rangle^2\langle 53|\Lambda\rangle^2 d_\Lambda\\ &\qquad\times[\textstyle\sum_i M_i^2\hbar^2(2\hbar\omega_i)^{-1}\coth(\hbar\omega_i/2kT)] ,\\ &\mathfrak{C}_0(\Lambda) = \tfrac{1}{4} g\langle T_2|{}^3A_2\rangle^2\langle 53|\Lambda\rangle^2 c_\Lambda\\ &\qquad\times[\textstyle\sum_i M_i^2\hbar^2(2\hbar\omega_i)^{-1}\coth(\hbar\omega_i/2kT)] ,\\ &w_\Lambda^0 = \langle\Lambda\lambda|\mathcal{H}_e^0(\vec{R}_0)|\Lambda\lambda\rangle ,\\ &\epsilon = \textstyle\sum_\Lambda \mathfrak{D}_0(\Lambda) w_\Lambda^0/\sum_\Lambda \mathfrak{D}_0(\Lambda) ,\end{aligned} \tag{22}$$

where the origin of energy in w_Λ^0 is arbitrary, we have put $\langle T_2\alpha|\mu_z|T_2\alpha\rangle = -gM_S$, and the $O(\kappa)$ terms in $\mathfrak{C}_1^{\nu 0}$ have been neglected.

Formally identical results are obtained if the active vibrations are supposed entirely a_{2u}, e_u, or t_{2u} (a_{1u} modes are easily shown to give zero intensity in our treatment). Choosing the M_i^2 constants appropriately leaves d_Λ identical to Eqs. (21) for all symmetries; c_Λ is then multiplied by -2, $+1$, and -1 for a_{2u}, e_u, and t_{2u} symmetries, respectively.

Equations (22) yield $\mathfrak{D}_0$, $\mathfrak{C}_0$, and $\mathfrak{C}_1^{\nu 0}$ values all proportional to one parameter, $\sum_i M_i^2\hbar^2(2\hbar\omega_i)^{-1}\coth\times(\hbar\omega_i/2kT)$. In the case that only one species of vibration is active, these quantities should then have identical T dependence in all bands and $\mathfrak{C}_0/\mathfrak{D}_0$ and $\mathfrak{C}_1^{\nu 0}/\mathfrak{D}_0$ ratios should be T independent.

In Table II, we give $\mathfrak{D}_0(A)$, $\mathfrak{C}_0(A)$, $\mathfrak{D}_0$, $\mathfrak{C}_0$, and $\mathfrak{C}_1^{\nu 0}$ values obtained from the ligand-field calculation and Eqs. (22), using[12] $g = 2.2145$ and assuming only t_{1u} modes to be active. We assume the lowest ^1E and $^1T_1$ to be within the $^3T_1^a$ and $^3T_1^b$ bands, respectively. The results agree semiquantitatively with the experimental results in Table I. From the above discussion it follows that this would also be the case if e_u modes were assumed active. On the other hand, there would be total lack of agreement if a_{2u} or t_{2u} symmetries were involved. Any appreciable contribution from the latter can therefore be discounted. If it is assumed that the $d \rightarrow d$ transition moments arise from nearest-neighbor nuclear displacements alone, atoms further distant giving negligible contribution, e_u modes are also eliminated since the NiO_6 cluster participates only in t_{1u} and t_{2u} phonons. If more distant shells are taken to be important, then e_u contributions could also be present. However, these are very unlikely to approach the contributions of t_{1u} phonons involving nearest-neighbor ions.

The consistent over-all agreement provides support for the ligand-field calculation. This shows conclusively that the $^1\Gamma$ band is entirely $^1T_2$, the calculated $\mathfrak{D}_0$ and $\mathfrak{C}_0$ values for $^1A_1$ being negligible in comparison. The highest ^1E, $^1T_2$, and $^1A_1$ states are calculated to have absorption and MCD intensities one to two orders of magnitude lower than the observed $^1T_2$. These would be detectable in MCD but not absorption with our crystal. Careful searching at 11 °K and 50 kG up to the accessible limit (~ 30 000 cm^{-1}) yielded no additional bands and these states are reliably assumed to be higher in energy, as calculated. No obvious sign of the $^1T_1$ state is detected either; this state is presumably inside, and broadened by, the $^3T_1^b$ band. The calculations suggest the lowest ^1E level to lie within the $^3T_1^a$ band. Evidence for its presence is discussed below.

Further confirmation of our treatment is provided by the experimental T dependence of the $^3T_1^a$ and $^3T_1^b$ $\langle A\rangle_0$ values, which are nearly identical, as predicted. Insufficient data are obtained to check the T independence of $\mathfrak{C}_0/\mathfrak{D}_0$ and $\mathfrak{C}_1^{\nu 0}/\mathfrak{D}_0$ values.

The agreement with experiment is not exact, and several probable reasons can be invoked. In the calculations of $\vec{m}_i^{\alpha\lambda}$ we ignored states other than $^3A_2$ in the ground state; however, the $^3T_2$ coefficient is ~ 0.1 and hence terms involving $^3T_2$ are not necessarily negligible. Borrowing of $^3A_2 \rightarrow {}^3T_2$ vibration-induced intensity by other transitions through spin-orbit coupling should probably not be entirely ignored. The use of a single average energy W_T^0 can be criticized; if the lowest charge-transfer states are important in generating intensity, these are probably sufficiently low to make $W_{^3T_1^b}^0 - W_X^0$ significantly smaller than $W_{^3T_1^a}^0 - W_X^0$. Inclusion of this difference would increase the $^3T_1^b$-to-$^3T_1^a$ intensity ratio. The ligand-field parameters can also be varied to some extent, changing the calculated parameters. On the experimental side, the background problems in both $^1T_2$ and $^3T_1^b$ bands make errors likely in their absorption moments. Different discrepancies are attributable to different errors. The disagreement in $\langle A\rangle_0$ ratios of the $^3T_1^a$ and $^3T_1^b$ bands is most likely due to the single-average-energy approximation. The disagreement in $\mathfrak{C}_0/\mathfrak{D}_0$ for $^3T_1^a$ is attributable to inadequate treatment of second-order spin-orbit effects. For both $^3T_1^a$ and $^3T_1^b$ bands, $\mathfrak{C}_0 = 0$ in the first-order approximation (in which mixing of states within a band with those outside is neglected) and nonzero $\mathfrak{C}_0$ values only arise to higher order. In view of the neglect of $^3T_2$ mixing into the ground state, the agreement for $^3T_1^b$ is more surprising than the disagreement for $^3T_1^a$. We note, however, that this does not apply to the $\mathfrak{C}_0$ values for the spin-forbidden bands, and the agreement for the $^1T_2$ band is not fortuitous. The discrepancies in the $\mathfrak{C}_1^{\nu 0}/\mathfrak{D}_0$ values for the $^3T_1$ bands are probably also due to the approximations in treating the spin-orbit coupling.

We turn now to consider the fine structure of the $^3T_1^a$, $^3T_1^b$, and $^1T_2$ absorption bands. Following the discussion above all features must be vibration induced and magnetic dipole transitions can be ignored. It is immediately apparent from Figs. 2, 4, and 6 that a structure containing two main peaks, spaced some 200 cm^{-1}, occurs in all of the bands. This must therefore be vibrational in origin. The $^3T_1^a$ band shows four such structures at relative energies at 8 °K of 0, ~ 400, 1030, and 1480 cm^{-1}. These spacings closely reproduce the calculated relative spin-orbit energies of 0, 416, 1062, and 1145 cm^{-1} (Table II) and each band can thus be firmly attributed to a single spin-orbit component. The $^1T_2$ band shows one such structure consistent with its assignment to a single spin-orbit level. The low-energy region of the $^3T_1^b$ band also exhibits this band shape but it is not clearly repeated as in the $^3T_1^a$ band. This can be attributed to the smaller spin-orbit coupling, giving greater overlap and smearing out of the vibrational structure.

We assign the vibrational structure principally to single-quantum excitations of t_{1u} phonons, for several reasons. First, since the contributions of one- and two-electron excitations to the excited states vary considerably, if the structure were due to potential surface changes substantially different shapes would be expected in different bands. Sec-

ond, the Sangster-McCombie calculations[13] of vibronic sidebands in emission from both V^{2+} and MgO : Ni^{2+} due to one-phonon t_{1u} excitations gave double-peaked shapes strikingly similar to those observed in our absorption spectra. In particular, in both calculations and experiment, the main peaks occur about 200 cm^{-1} apart and slight structure is displayed therein. The calculated peaks occur at ~ 200 and ~ 400 cm^{-1} above the zero-phonon transition. This interpretation then leads to placement of zero-phonon energies ~ 200 cm^{-1} below the first peak of each vibrational structure. Support for this is provided by the observation of hot bands that appear and intensify with increasing T to the red of each band (Figs. 2, 4, and 6). The peak first to appear and most intense is in all three bands 360–400 cm^{-1} lower than the first "cold" vibrational peak. The simplest interpretation is that the hot bands are mirror images in energy of the cold bands, reflected about the zero-phonon transition lying 180–200 cm^{-1} below the first "cold" peak, as would occur precisely if the ground- and excited-state potential surfaces were identical. Third, the effective allowing frequencies obtained from the $^3T_1$ band $\langle A \rangle_0$ values (Fig. 8) are in the same region as the average frequency of the vibronic profile.

The remaining broadening and structure is then associated with differences in ground- and excited-state potential surfaces. We have no quantitative evidence relating to either the magnitude of such changes or the relative importance of totally symmetric and nontotally symmetric distortions. Qualitatively, the absorption spectra show no obvious sign of Jahn-Teller effects in the $^3T_1^a$, $^3T_1^b$, or $^1T_2$ states and the absence of any substantial Jahn-Teller effect in the $^3T_1^a$ level seems especially clear from the agreement of calculated and observed spin-orbit splittings.

The MCD dispersion can also be satisfactorily interpreted qualitatively without consideration of Jahn-Teller effects. When these are absent, the rigid-shift (RS) approach[7] is valid and each electronic transition can be considered separately, even when the corresponding absorption bands overlap. The MCD of a band is then the sum of $\mathfrak{A}$, $\mathfrak{B}$, and $\mathfrak{C}$ terms, with moments given by Eqs. (2) and (9). The principal features of the observed MCD can be interpreted in terms of $\mathfrak{A}$ and $\mathfrak{C}$ terms due, respectively, to Zeeman shifts and population changes in ground-state Zeeman levels. As the temperature decreases, the latter increase and the MCD of each spin-orbit transition tends to the shape of the corresponding absorption, but with a sign dictated by $\mathfrak{C}_0(\Lambda)$, given by Eqs. (22). Thus the first two components of $^3T_1^a$ have positive $\mathfrak{C}_0$ values, as expected for A_1 and T_1 excited states, while the last two components are of opposite sign, also as predicted. The $^1T_2$ band and the lowest (E) $^3T_1^b$ component conform similarly to expectation. As T increases changes in shape occur, most noticeably in the sharper features, corresponding qualitatively to the increasing relative importance of MCD with derivative dispersion and hence attributable to $\mathfrak{A}$ terms. The sign of the $\mathfrak{A}$ terms can be calculated trivially for the lowest A_1 and E components of $^3T_1^a$ and $^3T_1^b$, respectively, since here $\langle J_\lambda | \mu_z | J_{\lambda'} \rangle = 0$ and $\mathfrak{A}_1 = \mathfrak{C}_0$. Equations (21) and (22) predict negative and positive contributions to $\langle \Delta A \rangle_1^{\nu 0}$ for A_1 and E states, respectively, as is observed. We have not attempted a quantitative evaluation of the RS model. However, the qualitative agreement with experiment further supports the conclusion that Jahn-Teller effects are at most small.

The $^3T_1^a$ absorption band differs from the $^1T_2$ and $^3T_1^b$ bands in having a distinct plateau to the red of the first strong transition. Also, the second spin-orbit component is much less sharply resolved than the other three. Either, or both, of these features may be due to the ^1E level. The low-energy absorption agrees well with the predicted energy (Table II), but the latter is sensitive to the ligand-field parameters used (especially C) and definite identification cannot be claimed from this alone.

Our ligand-field parameters can be varied somewhat, without significantly affecting the fit to the experimental data. Determination of optimum parameters requires both a more complete analysis of the band shapes, giving precise vertical excitation energies, and identification of more singlet states.

Various studies of MgO : Ni have been published previously. Kröger, Vink, and Boomgaard[14] reported absorption and emission features, without analysis. Low[15] obtained and assigned room temperature and 77 °K absorption spectra. The $^3T_2$, $^3T_1^a$, $^3T_1^b$, and $^1T_2$ bands were correctly assigned, except that the splitting of the $^3T_1^a$ band was attributed to overlap with the ^1E level. However, the three bands observed above $^3T_1^b$, assigned to the higher singlet states, are not seen in our spectra. These may be ion-cluster transitions (analogous to those observed[16] in $KMgF_3$: Ni), since the crystals were very inhomogeneous, or due to impurities. In either case, their assignment requires more study and the identification of the higher singlet states cannot be taken as definite.

Pappalardo, Wood, and Linares[6] (PWL) reported low-temperature spectra on crystals more dilute than ours by an order of magnitude and only the spin-allowed bands were clearly observed. Our results are in essential agreement for these bands. PWL also attempted to correlate spin-orbit states with observed peaks. Rather different interpretations were arrived at; in particular, the double-peaked structure was in several cases assigned to electronic splitting rather than vibrational struc-

ture. Our results appreciably modify their analysis.

More recently Ralph and Townsend[17,18] (RT) have reported absorption and emission spectra. Their absorption spectra include the $^1T_2$ band and are in good agreement with ours. However, the analyses differ considerably. RT assign the highest-energy "cold" peak in the $^1T_2$ emission to the zero-phonon magnetic dipole transition. This lies 400 cm^{-1} below the first "cold" peak in absorption. The rest of the emission is then assigned to vibronic sidebands. However, the emission spectrum is very close to a mirror image of the absorption. Further, since the electric dipole vibration-induced intensity is much larger than the magnetic dipole intensity in absorption, this should also be the case in emission. Finally, the highest-energy peak in emission coincides with the hot band observed in our absorption spectra. Hence the emission can only be assigned as vibration-induced electric dipole sidebands to a zero-phonon line 200 cm^{-1} higher than the highest emission peak, and 200 cm^{-1} lower than the lowest absorption peak, the position deduced earlier. It follows that the identification by RT of combinations of 170- and 230-cm^{-1} vibrational intervals is not meaningful. Also, there is then no justification for attributing structure in the first emission peak to a Jahn-Teller effect, this more likely arising from the t_{1u} phonon dispersion (such a splitting is clearly visible in the Sangster-McCombie calculations for MgO:Ni). Less complete analyses of the $^3T_1^a$ and $^3T_1^b$ bands were also attempted. Again, the identification of 170- and 230-cm^{-1} vibrational intervals is to be regarded with suspicion. It is also worth noting that the 13 000-cm^{-1} emission band has a very complex shape, which is not expected if due to just a single $^3T_1^a$ (or ^1E)$\rightarrow{}^3A_2$ transition, and that emission to $^3A_2$ is observed from both $^1T_2$ and $^3T_2$. The former band also coincides with the $^1T_2\rightarrow{}^3T_2$ interval and this appears to be a possible alternative assignment for the emission. The involvement of several electronic components and of two excited-state manifolds could easily lead to a band shape quite different from those terminating in the ground state. Finally, the magnetic dipole intensities calculated by RT are considerably in error (and generally too large) owing to neglect of the effect of spin-orbit coupling on the ground state.

PWL and RT also discuss the $^3T_2$ band which is observed in both emission and absorption. Further comments on this band have been made by Sturge,[19] favoring some Jahn-Teller activity in the $^3T_2$ state, and the Sangster-McCombie calculations also referred to this band. We are currently carrying out MCD experiments in this region which should enable this situation to be clarified and therefore refrain from further analysis here.

Also relevant is the recent MCD study of Ni $(BrO_3)_2\cdot 6H_2O$.[20] Both absorption and MCD have obvious similarities to the MgO:Ni results, although much less fine structure is resolved owing to the more complex electronic and vibrational situations. Harding *et al.* interpreted their data using the rigid-shift approach and also arrived at the conclusion that essentially t_{1u} vibrations were active.

V. CONCLUSION

Absorption moments have been discussed previously for vibration-induced transitions (especially the zeroth moment), as also have MCD and absorption moments for allowed transitions.[2,4] However, no MCD moment analysis has previously been carried out for vibration-induced bands and our treatment thus extends the scope of MCD theory. The results show that, as for allowed transitions, even for broad bands the zeroth and first moments can provide directly information on excited-state symmetries, wave functions, and electronic splittings. In addition, information on the symmetry of the vibrations causing the intensity can be obtained. In principle, higher moments can also yield results relating to excited-state potential surface changes from the ground state. Such analysis is more complex than for allowed transitions and has not been discussed explicitly in this paper.

We have been able to improve the characterization of the $^3T_2$, $^3T_1^a$, $^3T_1^b$, and $^1T_2$ absorption bands in MgO:Ni. Moment analysis of absorption and MCD together confirms the ligand-field analysis, shows that the $^3T_1^a$, $^3T_1^b$, and $^1T_2$ bands are entirely vibration induced, and leads to the conclusion that the phonons involved are at least predominantly t_{1u}. Consideration of the absorption and MCD band shapes leads to a reasonable over-all interpretation of the structures of the $^3T_1^a$, $^3T_1^b$, and $^1T_2$ bands. It is concluded that the main vibrational structure arises from the allowing t_{1u} mode dispersion and that the excited states are little distorted from the ground state. The $^3T_1^a$ spin-orbit components are clearly identified and there appears to be no reason to invoke Jahn-Teller effects in any of these states.

Further work on MgO:Ni is indicated in a number of areas: Band-shape calculations with realistic phonon spectra are needed for the $^3T_1^a$, $^3T_1^b$, and $^1T_2$ bands to confirm (or disprove) our analysis and, ideally, evaluate the excited-state geometries and potential surfaces. Moment analysis, including second and third moments, may be useful in conjunction with such calculations to place limits on parameters involved. Further study of the $^3T_2$ band is needed and is under way. Work with more concentrated, thinner crystals would be useful in looking for the weak spin-forbidden transitions not observed so far. Further study of the emission, particularly the 13 000-cm^{-1} band, is required to identify

the states involved and provide further data for comparison with band shape calculations. Experiments with very dilute crystals to look at the charge-transfer bands at higher energy and on concentrated or pure NiO crystals to study cooperative phenomena would also be of interest. Finally, theoretical calculations are needed to explain the various features of the interaction between Ni^{2+} and a surrounding MgO lattice. This includes the ligand-field parameters, the ground- and excited-state potential surfaces, and the vibration-induced transition probabilities.

Our work shows that broad vibration-induced transitions are not too complex to be usefully studied by MCD. Many such transitions are known, especially in transition-metal spectroscopy, and MCD should prove a potent tool in their further investigation. We are currently studying other ions in MgO and $KMgF_3$ and will report our results in future publications.

ACKNOWLEDGMENTS

We are deeply grateful to Cary Instruments, and especially to Dr. J. J Duffield and Dr. A. Abu-Shumays, for their interest and collaboration in this work. We also thank Professor D. A. Dows for the use of a helium Dewar, A. Mann for assistance with some experiments, the National Institutes of Health and the Alfred P. Sloan Foundation for grants (to P. J. S.), and the Fulbright-Hays Program for a travel grant (to G. A. O.).

---

*Alfred P. Sloan Foundation Fellow.

[1]P. N. Schatz and A. J. McCaffery, Quart. Rev. Chem. Soc. 23, 552 (1969).

[2]C. H. Henry and C. P. Slichter, in *Physics of Color Centers*, edited by W. B. Fowler (Academic, New York, 1968), p. 351.

[3]J. Ferguson, Progr. Inorg. Chem. 12, 159 (1970).

[4]G. A. Osborne and P. J. Stephens, J. Chem. Phys. (to be published).

[5]Cary Instruments, 2724 South Peck Road, Monrovia, Calif. 91016.

[6]R. Pappalardo, D. L. Wood, and R. C. Linares, J. Chem. Phys. 35, 1460 (1961).

[7]P. J. Stephens, J. Chem. Phys. 52, 3489 (1970).

[8]When, with Eq. (6), $\langle a|\mu_z|a'\rangle = \langle A_\alpha|\mu_z|A_\alpha\rangle \delta_{aa'}$ as required for Eq. (3) to hold.

[9]Since in this paper we only discuss the $d^8 Ni^{2+}$ states the g symmetry labels are dropped.

[10]The ligand-field program was written by B. D. Bird and is described in B. D. Bird, Ph.D. thesis (Oxford University, 1969) (unpublished).

[11]Insufficient $\langle A\rangle_0$ values were obtained for the $^1T_2$ band to warrant fitting.

[12]S. R. P. Smith, F. Dravnieks, and J. E. Wertz, Phys. Rev. 178, 471 (1969).

[13]M. J. L. Sangster and C. W. McCombie, J. Phys. C 3, 1498 (1970).

[14]F. A. Kröger, H. J. Vink, and J. van den Boomgaard, Physica 18, 77 (1952).

[15]W. Low, Phys. Rev. 109, 247 (1958).

[16]J. Ferguson, Aust. J. Chem. 21, 323 (1968).

[17]J. E. Ralph and M. G. Townsend, J. Chem. Phys. 48, 149 (1968).

[18]J. E. Ralph and M. G. Townsend, J. Phys. C 3, 8 (1970).

[19]M. D. Sturge, Solid State Phys. 20, 91 (1967).

[20]M. J. Harding, S. F. Mason, D. J. Robbins, and A. J. Thomson, Chem. Phys. Letters 7, 70 (1970).